Journal of Materials Chemistry A

ROYAL SOCIETY OF CHEMISTRY

PAPER

View Article Online
View Journal | View Issue

Cite this: J. Mater. Chem. A, 2025, 13, 31202

Taming of 3,4-di(nitramino)furazan II:high-energy coordination complexes with exceptional catalytic activity for the thermal decomposition of ammonium perchlorate

Jizhou Dong,†[a] Jinchao Ma, †*[a] Shuyue Xu, [a] Xingyang Cui,[a] Hua Qian*[a] and Jean'ne M. Shreeve *[b]

Received 14th May 2025
Accepted 16th August 2025

DOI: 10.1039/d5ta03900b

rsc.li/materials-a

3,4-Di(nitramino)furazan (**DNAF**) offers advantages like simple synthesis, high oxygen content (42.1%), and strong detonation (D = 9376 m s^{-1}, P = 40.5 GPa), but suffers from low thermal stability (T_d = 99 °C) and mechanical sensitivity (IS < 1 J, FS < 5 N). In this study, we designed a series of Co(II) and Ni(II) energetic complexes (**ECP-1** to **ECP-8**, (energetic catalyst for propellant) based on it, which showed improved thermal stability (T_d = 239.5–253.0 °C) and reduced sensitivity (IS ≥ 10 J, FS ≥ 172 N), along with high energy content (D = 7345–8041 m s^{-1}, P = 21.83–32.0 GPa). Evaluation through TG-DSC revealed that just 2 wt% of these complexes could lower the decomposition temperature of ammonium perchlorate (AP) effectively by 48.11–119.33 °C, reduce its activation energy by 110.65–156.10 kJ mol^{-1}, and increase combustion rate by 14–38%. This study provides insights into stabilizing **DNAF** through coordination complexes, with potential applications as combustion additives for solid propellants.

Introduction

N-Heterocycles exhibit notably high positive heats of formation, rendering them highly advantageous as precursors for synthesizing a diverse array of energetic compounds.[1–5] Recent studies have highlighted advances in the synthesis of oxadiazole-based energetic compounds, which exhibit considerable structural diversity and elevated energy characteristics.[6–10] Furthermore, a positive correlation has been observed between increased nitrogen and oxygen content and enhanced performance outcomes.[11] Di(nitramino)-oxadiazole ($C_2H_2N_6O_5$), characterized by a nitrogen and oxygen content of 86.3%, possesses four theoretically possible isomers: 3,4-di(nitramino)furazan (**DNAF**), 2,5-di(nitramino)-1,3,4-oxadiazole, 3,5-di(nitramino)-1,2,4-oxadiazole and 4,5-di(nitramino)-1,2,3-oxadiazole. **DNAF**, the only isomer documented in the literature, exhibits exceptionally high detonation performance (D = 9376 m s^{-1}, P = 40.5 GPa) but very low mechanical sensitivity (IS < 1 J, FS < 5 N) and limited thermal stability (T_d = 99 °C).[12] The contradiction between energy and stability has resulted in **DNAF** exhibiting subpar safety characteristics, thereby posing a significant hindrance to its extensive utilization in the realm of energetic materials.

The implementation of bridging units may enhance the stability of energetic materials,[13–16] and an explanation for this phenomenon can be located in the subsequent reports (Fig. 1). 1,4- Dinitrofurazano[3,4-b]piperazine (A), which incorporates an ethylene group into its conjugated system, exhibits decomposition at a temperature of 134 °C.[17,18] In contrast, 1,4,5,8-tetranitroazadi furazano[3,4-c][3,4-h]decaline (B), which contains two unstable **DNAF** units sharing a single ethylene group, demonstrates thermal sensitivity with a decomposition temperature of 70 °C. 4,6,8-Trinitro-4,5,7,8-tetrahydro-6H-furazano-[3,4-f]-1,3,5-triazepine (C), which features an *N*,*N*-diethylnitramide bridge, exhibits superior thermal stability (T_d = 150 °C) compared to **DNAF**.[19] Another way to improve the thermal stability and mechanical safety of energetic compounds is making salts. This is evidenced by the properties of various **DNAF** salts, including diammonium (D, T_d = 191 °C, IS = 8 J, FS = 240 N), dihydrazium (E, T_d = 206 °C, IS = 12 J, FS = 160 N), and dihydroxylammonium (F, T_d = 181 °C, IS = 5 J, FS = 120 N) salt.[12]

Drawing upon the findings related to energetic salts, we have shifted our focus towards the exploration of energetic complexes to enhance the potential applications of **DNAF**. Energetic complexes, a category of novel energy materials characterized by their adjustable structures and controllable properties, have garnered considerable attention since their initial introduction.[20,21] Recent studies have identified Fe(II) tetrazine complexes characterized by low mechanical sensitivity and elevated initiation thresholds as potential candidates for secondary explosives in near-infrared

[a]School of Chemistry and Chemical Engineering, Nanjing University of Science and Technology, Nanjing, 210000, China. E-mail: mjinchao@njust.edu.cn

[b]Department of Chemistry, University of Idaho, Moscow, Idaho, 83844-2343, USA. E-mail: jshreeve@uidaho.edu

† J. Dong and Dr J. Ma contributed equally.

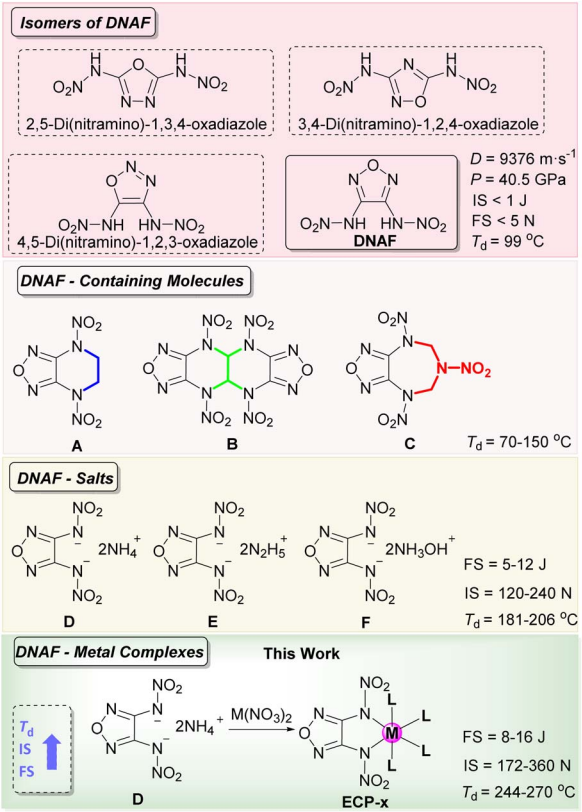

Fig. 1 Energetic derivatives from DNAF.

(NIR) optical initiation systems.[22] Furthermore, energetic complexes have been extensively documented as combustion catalysts, attributed to their relatively active electron configurations, diverse valence states, and available electron orbitals.[23–27] In particular, the transition metals, cobalt and nickel, exhibit remarkable catalytic properties and are extensively utilized in the catalytic thermal decomposition of ammonium perchlorate.[28–32]

This study focuses on the optimization of energy and sensitivity in **DNAF** through ligand regulation strategies. A series of energetic complexes were synthesized by manipulating the reaction conditions, utilizing **DNAF** as the main ligand and Co(II)/Ni(II) as the active metal centre. Structural characterization and performance evaluations of these metal complexes were conducted, revealing that they possess commendable safety and energetic characteristics. Subsequent investigations into the catalytic thermal decomposition of AP and the combustion rate of the propellant demonstrated the exceptional catalytic capabilities of these complexes. Consequently, these energetic complexes are identified as promising candidates for solid propellant energetic promoter, as they effectively regulate the thermal decomposition temperature of AP while significantly enhancing the energy output of the propellant.

Results and discussion

Synthesis and structural characterization

Based on the existing literature,[12] the **DNAF** ammonium salt was synthesized as a precursor, and a variety of energetic complexes utilizing **DNAF** as a ligand were subsequently developed. $Co(NO_3)_2\cdot 6H_2O$ or $Ni(NO_3)_2\cdot 6H_2O$ was dissolved in 1 mL of distilled water and subsequently introduced into an aqueous solution of **DNAF** ammonium salt at a temperature of 60 °C. The resulting reaction mixture was stirred at this temperature for a duration of 2 hours, yielding solutions of [Co(**DNAF**)$(H_2O)_4$] (designated as **ECP-1**) or [Ni(**DNAF**)$(H_2O)_4$] (designated as **ECP-5**). Following this, a solution of $NH_3\cdot H_2O$, ethylenediamine (EDA), carbohydrazide (CHZ), or formyl hydrazine (FHZ) was added to the aforementioned solution, respectively. The reaction mixture was again stirred at the same temperature for an additional 2 hours. Upon cooling to room temperature, the precipitate was filtered, washed with cold water, and dried at 50 °C, resulting in the formation of solids: [Co(**DNAF**)$(NH_3)_3$(H_2O)] (**ECP-2**), [Co(**DNAF**)$(EDA)_3$] (**ECP-3**), [Co(**DNAF**)(FHZ)(H_2O)] (**ECP-4**), [Ni(**DNAF**)$(NH_3)_4$] (**ECP-6**), [Ni(**DNAF**)$(EDA)_3$] (**ECP-7**), and [Ni(**DNAF**)$(CHZ)_3$] (**ECP-8**), respectively (Fig. 2). The comprehensive procedures are illustrated in the SI.

Crystallization of **ECP-1** to **ECP-8** from hot water yields colourful blocks suitable for single-crystal X-ray measurement (Fig. 3 and S1–S8). Two types of crystal structures have been identified: **ECP-1**, **ECP-2**, **ECP-4**, **ECP-5**, and **ECP-6** belong to a class of complexes where the **DNAF** anion participates in coordination, whereas **ECP-3**, **ECP-7**, and **ECP-8** constitute

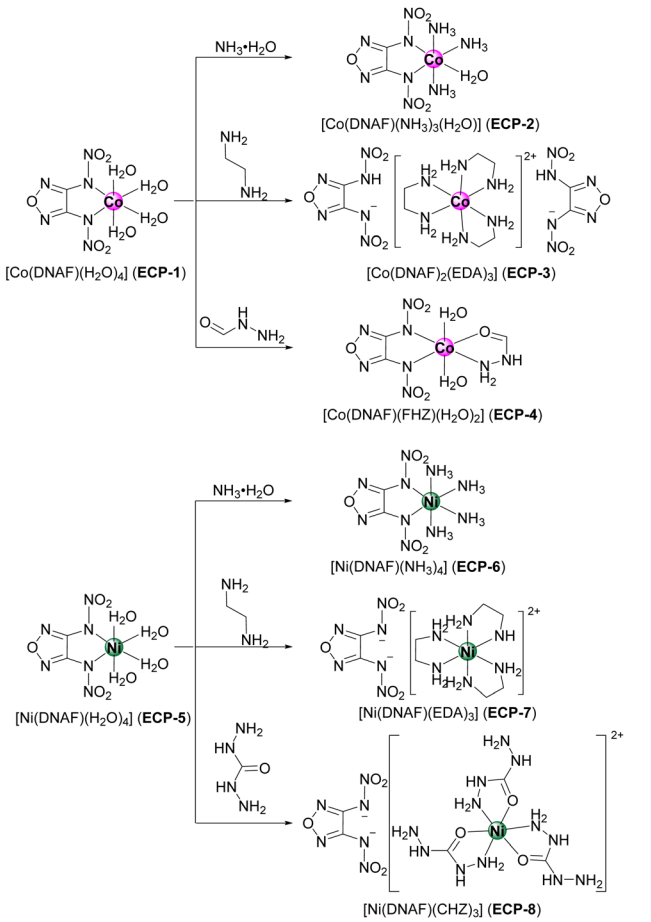

Fig. 2 Synthesis route of ECP-1 to ECP-8.

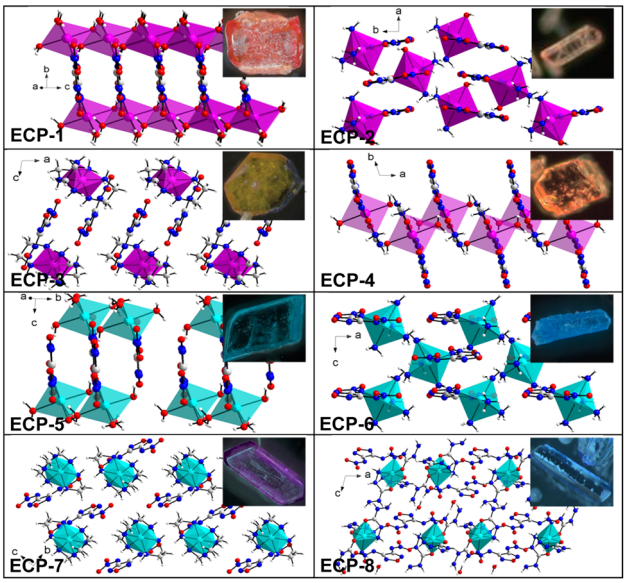

Fig. 3 Digital microscope images of single crystals and packing diagrams of ECP-1 to ECP-8.

a separate class where the **DNAF** anion is free from coordination. Single-crystal diffraction results indicate that crystals of **ECP-1**·$4H_2O$, **ECP-2** and **ECP-8**·H_2O formed in the $P2_1/n$ monoclinic space group, and the calculated densities of 1.852–2.038 g cm^{-3} at 173 K. Crystals of **ECP-4**·H_2O, **ECP-5**·$4H_2O$, and **ECP-7** belong to the *P*-1 triclinic space group, with calculated densities ranging from 1.614 to 2.095 g cm^{-3} at 173 K. Crystals of **ECP-3**·$2.5H_2O$ (ρ = 1.770 g cm^{-3}) and **ECP-6** (ρ = 1.976 g cm^{-3}) formed in the *C*2/*c* in monoclinic and $Pna2_1$ in orthorhombic space group, respectively.

In the structure of **DNAF**-coordinated complexes (**ECP-1**, **ECP-2**, **ECP-4**, **ECP-5**, **ECP-6**), despite the addition of an excess of the **DNAF** ligand source, only one molecule of **DNAF** engaged in the coordination process, potentially due to steric hindrance effects. In both **ECP-1** and **ECP-5**, the metal atom coordinates with two nitrogen atoms linked to the nitro group in **DNAF** (**ECP-1**, Co(1)–N(1) = 2.128(2) Å, Co(1)–N(3) = 2.147(2) Å; **ECP-5**, Ni(1)–N(2) = 2.101(3) Å, Ni(1)–N(5) 2.079(3) Å), along with four H_2O molecules (**ECP-1**, O(9)–Co(1)–O(8) = 177.74(9)°; O(7)–Co(1)–N(1) = 173.39(9)°; O(6)–Co(1)–N(3) = 172.61(9)°; **ECP-5**, O(1)–Ni(1)–O(2) = 90.63(9)°, O(1)–Ni(1)–O(3) = 86.99(9)°, O(1)–Ni(1)–O(4) = 89.40(9)°), collectively forming an irregular octahedral structure. Following the treatment of **ECP-5** with ammonia, all four H_2O ligands within the structure are effectively replaced, yielding **ECP-6**. Conversely, in the case of **ECP-2** and **ECP-4**, there are still residual water ligands even when subjected to elevated temperatures and increased ligand's concentrations.

In the complexes discussed, Co(II) or Ni(II) engages with small molecules, including H_2O and NH_3, which leads to the formation of a cruciform configuration. This structural arrangement exhibits a head-to-foot orientation, contributing to a more compact packing, as demonstrated by the measurements of crystal density. However, in complexes **ECP-3**, **ECP-7** and **ECP-8**, it can be found that ethylenediamine and carbohydrazide possess exceptional metal coordination capabilities, enabling them to extract Co(II) or Ni(II) from **DNAF** effectively. The unbound planar **DNAF** is dispersed within an octahedral framework characterized by a loose structure and a low crystallinity coefficient, resulting in a reduction of its density.

To enhance our comprehension of the alterations in *N*-nitramine groups within **DNAF** prior to and following coordination, we conducted an analysis of inter/intramolecular interactions present in the **ECP-1** to **ECP-8**, subsequently comparing these interactions with those observed in **DNAF**. In the crystal structure of **DNAF**, the *N*-nitramines are twisted out of the furazan ring plane, and no hydrogen-bond interaction is observed between the nitro groups and H3/H8. This is considered one of the primary reasons for the material's unstable nature. As shown in Fig. S9, the *N*-nitramines and furazan ring in the crystals of **ECP-1** to **ECP-8** are distributed almost in the same plane, which is evidenced by the torsion angle of N–N–C–N (Table S2: **ECP-1** to **ECP-8**, 0.1–20°; **DNAF**, 127.2°). Furthermore, there is an augmentation in "soft" interactions (N···H/O···H) between the nitro groups and adjacent molecules. The trigger bond in these molecules is the N–N bond in the *N*-nitramine moiety. For these complexes, the bond lengths of N–NO_2 fall in the range of 1.309(5)–1.339(4) Å (Table S2), significantly shorter than that of **DNAF** (1.3784(5)–1.3797(6) Å). These facts can contribute to the stabilization of **DNAF**, and subsequent analyses have also indeed confirmed that when combined with metals, **DNAF** demonstrates enhanced thermal stability and superior mechanical safety.

Thermal stabilities

Differential scanning calorimetry (DSC) and simultaneous thermogravimetric analysis (TG) were employed to assess the thermal stability of the energetic complexes **ECP-1** to **ECP-8** in a nitrogen atmosphere (Fig. 4 and S26–S33). The analysis was conducted at a heating rate of 10 °C min^{-1}, over a temperature range of 50 to 500 °C. The decomposition of **ECP-1** to **ECP-8** occurred at temperatures exceeding 239.5 °C, which is significantly higher than that of **DNAF** (99 °C) and other documented molecules containing **DNAF** (A–F, T_d = 70–206 °C). Specifically, **ECP-6** is composed of four ammonia molecules functioning as ligands, and the temperature at which initial decomposition occurs has been recorded at 269.9 °C.

The DSC and DTG curves of **ECP-1**, **ECP-2**, **ECP-4**, **ECP-5**, **ECP-6** and **ECP-7** exhibit a decrease at approximately 150 °C, which is indicative of a heat absorption peak and notable reduction in mass. Based on the chemical structure, it is plausible to speculate that these heat absorption peaks do not correspond to the melting points of the complexes; instead, they may originate from the departure of water or ammonia molecules embedded within the structural lattice. **ECP-3** and **ECP-4** exhibit two distinct exothermic peaks, with the initial peak occurring around 240 °C, which is believed to correspond to the decomposition of the energetic anions. The subsequent decomposition noted at approximately 320 °C is attributed to the high thermal decomposition temperatures associated with

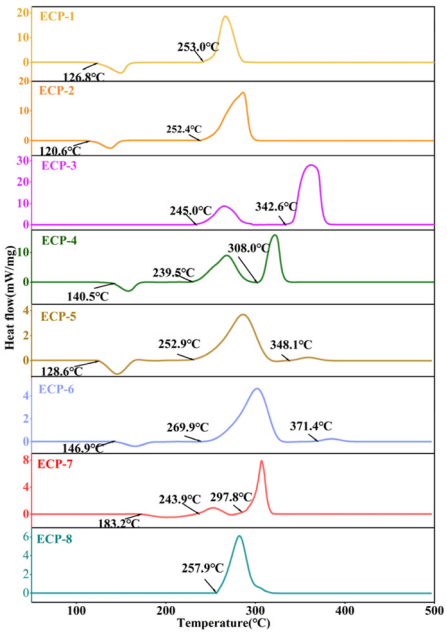

Fig. 4 DSC curves of ECP-1 to ECP-8.

the ligands, ethylenediamine and formyl hydrazine. The TG curves indicate a retention of mass (23.25–45.79%) following the decomposition of the complexes, which is believed to result from the transformation of the complexes into their respective oxides.

Energetic properties

In this paper, the detonation properties were calculated by EXPLO5 (version 6.01),[33] where the density was measured by a helium hydrometer at room temperature, and the enthalpy of formation was obtained from the standard molar heat of combustion in accordance with Hess's law. Additionally, the heat of combustion for the complexes was assessed at constant volume using oxygen bomb calorimetry. Comprehensive details regarding the calculation procedures are given in the SI. The density spans a precise range from 1.61 g cm^{-3} (**ECP-7**) to 2.11 g cm^{-3} (**ECP-4**). Among them, the formyl hydrazine-containing complex (**ECP-8**) has the highest density of 2.11 g cm^{-3} which is superior to most cobalt-based energetic complexes.[28–30,34–36] Based on the calculation results, the detonation velocity and detonation pressure of **ECP-1** to **ECP-8** fell within the ranges of 6618–8167 m s^{-1} and 16.2–32.0 GPa, respectively. It is readily apparent that **ECP-3** and **ECP-7**, coordinated with ethylenediamine, exhibit lower density subsequently impacting their detonation performance. The presence of water acts to absorb and dissipate the energy released during the detonation process of **ECP-1** and **ECP-5**, resulting in a decrease in detonation performance parameters. In **ECP-4**, the formyl hydrazine is aligned essentially in the same plane as **DNAF**$^{2-}$, leading to a denser internal molecular structure. So **ECP-4** demonstrates the optimal energetic performance, with a density of 2.11 g cm^{-3}, detonation velocity of 8041 m s^{-1} and a detonation pressure of 32.0 GPa.

Sensitivity test

For preliminary safety assessments, the mechanical sensitivities to impact (IS) and friction (FS) were evaluated in accordance with established BAM methodology. The collected sensitivity data are summarized in Table 1. The impact sensitivity of the complexes exceeds 10 J, while the friction sensitivity surpasses 172 N, representing a significant enhancement in comparison to **DNAF**. Among these newly synthesized energetic complexes, **ECP-5** featuring a four-coordinated structure demonstrates a relatively high sensitivity (IS = 8 J, FS = 192 N). These values are comparable to those of its precursor, diammonium 3,4-dinitraminofurazanate (*D*, IS = 8 J, FS = 240 N). The ethylenediamine-incorporated complex **ECP-3** exhibits the highest insensitivity, demonstrating acceptable sensitivity levels with an impact sensitivity of 16 J and a friction sensitivity of 360 N. The molecular structure and weak inter/intramolecular interactions are critical determinants of the thermal stability and mechanical sensitivity of energetic materials. The single-crystal structures of the complexes reveal that the presence of numerous inter/intramolecular interactions within the crystal lattice significantly enhances the strength of bond and mechanical susceptibility of **DNAF**. In particular, for **ECP-3**, **ECP-7**, and **ECP-8**, the **DNAF** anion exists in a free state,

Table 1 Physical and detonation properties of ECP-1 to ECP-8 compared with DNAF

Compd	T_d[a] [°C]	Tcr[b] [°C]	ρ[c] [g cm^{-3}]	ΔH_f[d] [kJ mol^{-1}]	D[e] [m s^{-1}]	P[f] [GPa]	IS[g] [J]	FS[h] [N]	ES[i] [J]
DNAF	99.0	—	1.90	286.9	9376	40.5	<1	<5	—
ECP-1	253.0	250.52	1.98	−770.1	7345	23.1	12	240	>20
ECP-2	252.4	249.15	2.04	−539.9	7898	21.8	10	172	>20
ECP-3	245.0	232.72	1.80	210.9	7772	23.1	16	360	>20
ECP-4	239.5	225.59	2.11	−940.0	8041	32.0	15	252	>20
ECP-5	252.9	213.03	1.98	−960.9	7136	21.8	8	192	>20
ECP-6	269.9	273.67	1.98	−621.5	7986	23.5	10	192	>20
ECP-7	243.9	283.55	1.61	−486.2	6618	16.2	10	240	1
ECP-8	257.9	255.58	1.89	−1019.7	8167	23.5	15	360	0.5

[a] Thermal decomposition temperature (onset) under nitrogen gas (DSC, 10 °C min^{-1}). [b] Thermal explosion critical temperature. [c] Density measured with a gas pycnometer (25 °C). [d] Calculated heat of formation. [e] Calculated detonation velocity. [f] Calculated detonation pressure. [g] Impact sensitivity. [h] Friction sensitivity. [i] Electrostatic sensitivity.

but the weak interactions between the **DNAF** anion and other ligands, which originate from nitrogen and oxygen atoms, contribute to its stability (Fig. S9). Further evaluation of the electrostatic spark sensitivity and thermal explosion critical temperature of the complex was undertaken. The results in Table 1 indicate that the electrostatic sensitivity of **ECP-1** to **ECP-6** all exceed 20 J, while that of **ECP-7** and **ECP-8** is 1 J and 0.5 J, respectively. The critical thermal explosion temperatures of all complexes range from 213.03 to 283.55 °C (Fig. S34). This indicates that the complex has good safety performance.

Hirshfeld surface analysis

To investigate the influence of weak inter/intramolecular interactions within the complexes on their thermal stability and mechanical susceptibility, Hirshfeld surface maps for **ECP-1** to **ECP-8** were generated utilizing the Crystal Explorer software, along with the corresponding two-dimensional fingerprint maps. The red dots and blue dots on the molecular surface represent the strong and short interactions between different moieties. Fig. 5 shows that the red dots are predominantly situated in proximity to the nitro groups and the coordinated water molecules, which may be attributed to the presence of strong hydrogen-bonding interactions. 2D fingerprints illustrate the interactions among various elements. It is widely recognized that "solid" O···O closed-shell interactions enhance sensitivity, whereas "soft" hydrogen-bonding interactions (N···H/O···H) serve to absorb mechanical stimuli, thereby augmenting the mechanical sensitivity of energetic materials.[37–39] The pair of spikes on the left side of the 2D fingerprints are hydrogen bonding interactions. The quantitative analysis of these weak interactions indicates that the hydrogen bonding contributions of **ECP-1** to **ECP-8** comprised 59.5%, 58.4%, 57.4%, 63.2%, 59.1%, 61.6%, 56.2%, and 65.2% of the total interactions, respectively. These values are significantly greater than the hydrogen bonding proportion observed in **DNAF** (34.9%). Furthermore, the percentage of O···O interactions observed in **ECP-1** to **ECP-8** is less than 10%, which is significantly lower than the 29.0% recorded for **DNAF**. The analysis of the Hirshfeld surface indicates that the series of complexes exhibit a greater prevalence of "soft" hydrogen-bonding interactions and a reduced presence of "solid" interactions in comparison to **DNAF**. This characteristic is beneficial for enhancing the thermal stability and mechanical sensitivity of the entire molecular structure.

Catalytic performance on AP thermal decomposition

We investigated the catalytic effects of catalysts with different loadings (2 wt%, 5 wt%, 10 wt%) on AP (Fig. S35). Comparative analysis revealed that the catalytic effect improved as the catalyst content increased; however, the enhancement in catalytic performance was not significant. Consequently, a mixture of 2 wt% catalyst and AP was employed for subsequent research in this study.

DSC measurements were conducted over the temperature range of 50–450 °C, employing various heating rates of 5, 10, 15, and 20 °C min^{-1} in a nitrogen atmosphere, to evaluate the catalytic efficacy of these complexes on the thermal decomposition of AP. Fig. S36 shows the DSC scans for pure AP and a composite mixture containing AP. Through comprehensive comparative analysis (Fig. 6 and Table S27), when only 2% of the **ECP-2** is incorporated into AP, it can lower the high-temperature decomposition temperature of AP by as much as 119.3 °C. Its catalytic performance can be comparable to, or even surpass, that of most of the reported energetic complexes (with a content ranging from 2% to 25% in AP). In general, the decomposition temperature of AP is related to the burning rate

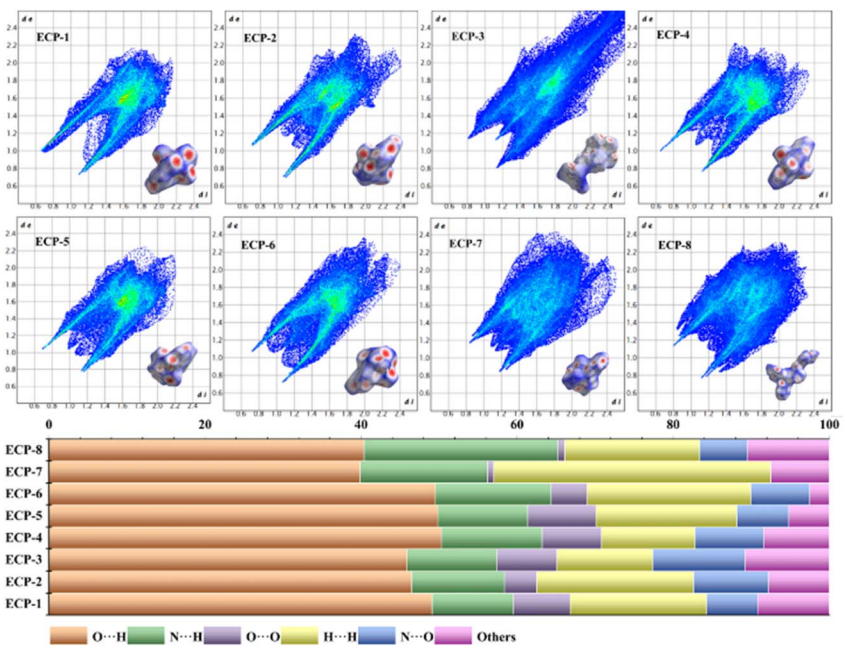

Fig. 5 Surface map and 2D fingerprint of **ECP-1** to **ECP-8** Hirshfeld (top); quantification of weak interactions of **ECP-1** to **ECP-8** (bottom).

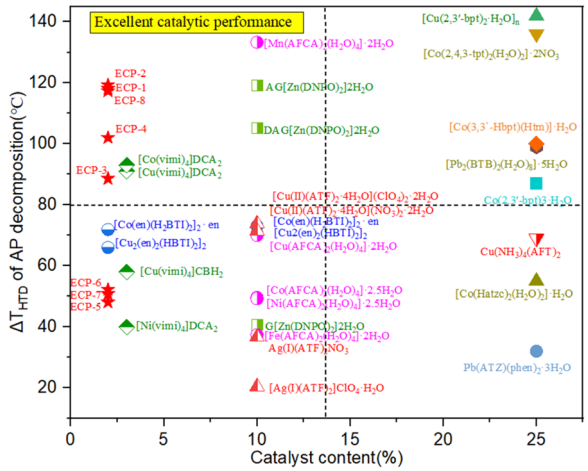

Fig. 6 Comparison of ECP-1 to ECP-8 with reported energetic catalysts.

of the composite solid propellants, which can be improved by shifting their peak temperatures (high temperature decomposition, HTD; low-temperature decomposition, Ltd) to the left and increasing their heat released during thermal decomposition with the burning rate catalysts.[40] The HTD at various heating rates were subjected to linear fitting using Kissinger eqn (1).[41] In this equation, T_p represents the peak temperature (K), β denotes the heating rate ($K\ min^{-1}$), R is the ideal gas constant ($8.314\ J\ mol^{-1}\ K^{-1}$), E_a signifies the apparent activation energy ($kJ\ mol^{-1}$) and A refers to the frequency factor. The parameters E_a and A can be determined using the Kissinger equation.

$$\ln(\beta/T_p^2) = \ln(AR/E_a) - E_a/(RT_p) \quad (1)$$

As shown in Fig. S36 and Table S27, these energetic complexes markedly reduce the activation energy of AP. In comparison to pure AP, the activation energies for the mixture of **ECP** with AP were reduced from 227.37 kJ mol^{-1} to 113.08 kJ mol^{-1} (**ECP-1**), 131.34 kJ mol^{-1}(**ECP-2**), 151.79 kJ mol^{-1}(**ECP-3**), 145.38 kJ mol^{-1}(**ECP-4**), 122.85 kJ mol^{-1}(**ECP-5**), 110.65 kJ mol^{-1}(**ECP-6**), 156.10 kJ mol^{-1}(**ECP-7**) and 122.37 kJ mol^{-1}(**ECP-8**), respectively. The activation energy of cobalt complexes (**ECP-1** to **ECP-4**) added system were comparable to those of nickel complexes (**ECP-5** to **ECP-8**). Theoretically, pre-exponential factor A and activation energy E_a are two independent variables, but Gallagher *et al.* first discovered the linear relationship between lnA and E_a in 1976, namely the kinetic compensation effect.[40] The E_a/lnA ratio serves as an indicator of the activity associated with the AP thermal decomposition reaction, with a lower ratio signifying enhanced reactivity. The ratio E_a/lnA for the mixtures of AP and **ECP-1** to **ECP-4** falls within the range of 7.11 to 7.86, which is lower than the corresponding values for **ECP-5** to **ECP-8** (7.49–9.72). Consequently, the catalytic activity exhibited by cobalt complexes surpasses that of the nickel series, particularly in the cases of **ECP-2** to **ECP-4**.

Application in HTPB-based propellant

To investigate the performance of the composite in practical applications further, a series of HTPB-based propellants were formulated. This propellant consisted of 66.0 wt% AP, 18.0 wt% nano-aluminum, 12.0 wt% hydroxyl-terminated polybutadiene (HTPB), 1.5 wt% 2,4-toluene diisocyanate (TDI), 0.5 wt% dibutyltin dilaurate (T12), and 2 wt% energetic complexes (**ECP-1** to **ECP-8**), respectively. Following the mixing of the aforementioned materials, the resultant solid propellant slurry was poured into a glass mold with an internal diameter of 9 mm, which had previously incorporated a bundle of nickel-chromium ignition wires at its base. The assembly underwent a vacuum treatment for 30 minutes and was subsequently cured at a temperature of 50 °C for 48 hours, resulting in the final HTPB-based solid propellant beam.

As illustrated in Fig. 7, upon ignition of the grain, the flame advanced uninterrupted to the terminal end of the grain across

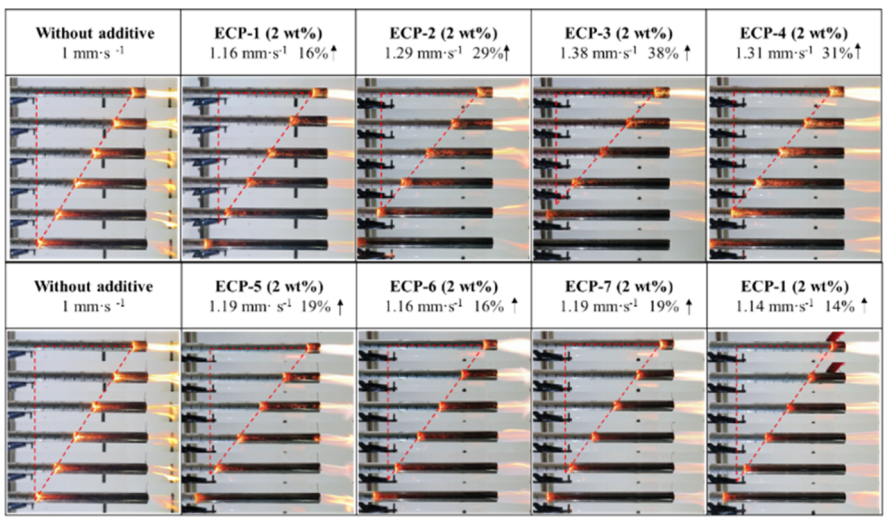

Fig. 7 Selected images of the burning of HTPB-propellant under atmospheric conditions.

all prepared propellant formulations. The HTPB-based propellant demonstrated stable and consistent combustion characteristics. HTPB propellant exhibits a stable and consistent combustion profile with the burning rate of 1.00 mm s^{-1} (without burn rate modifier). The introduction of **ECP-1** to **ECP-4** catalysts resulted in a significant increase in both flame lightness and burning rates, with recorded values of 1.16 mm s^{-1}, 1.29 mm s^{-1}, 1.38 mm s^{-1}, and 1.31 mm s^{-1} for the HTPB/AP/*n*Al/**ECP-1**, HTPB/AP/*n*Al/**ECP-2**, HTPB/AP/*n*Al/**ECP-3**, and HTPB/AP/*n*Al/**ECP-4** propellants, respectively. Nevertheless, slightly enhanced burning rates were observed (1.19 mm s^{-1} for HTPB/AP/*n*Al/**ECP-5**, 1.16 mm s^{-1} for HTPB/AP/*n*Al/**ECP-6**, 1.19 mm s^{-1} for HTPB/AP/*n*Al/**ECP-7**, and 1.14 mm s^{-1} for HTPB/AP/*n*Al/**ECP-8**, respectively). These rates correlated with their modest catalytic performance in the decomposition of AP. This correlation arose despite their demonstrated efficient catalytic activity in AP decomposition, as previously noted. The cobalt complexes **ECP-3** and **ECP-4** demonstrate remarkable catalytic efficacy, with **ECP-3** exhibiting the most significant enhancement in the burning rate of the propellant, achieving an increase of 38%.

Catalytic mechanism analysis

The experimental findings indicate that complexes containing cobalt atoms, specifically **ECP-1** to **ECP-4**, exhibit superior performance compared to the nickel series (**ECP-5** to **ECP-8**) in catalytic AP and propellant combustion, with **ECP-3** demonstrating the most significant efficacy. To further investigate the underlying mechanisms contributing to this performance disparity, we conducted theoretical calculations to simulate the catalytic process by using density-functional theory (DFT).[42–44] It is widely accepted that the primary reaction involved in the decomposition of AP in propellants can be represented by chemical eqn (2) and (3),[45]

$$NH_4^+ + ClO_4^- \rightarrow NH_3(s) + HClO_4(s) \rightarrow NH_3(g) + HClO_4(g) \quad (2)$$

$$NH_3 + 2O \rightarrow HNO + H_2O \quad (3)$$

The primary source of energy in the propellant is derived from the exothermic oxidation of metal and the generation of gases from the decomposition of AP. In the initial phase of the reversible reaction, the decomposition of ammonia (NH_3), which results from the breakdown of AP, acts as an inhibitory factor in the overall decomposition process. Therefore, accelerating the adsorption and consumption of NH_3 is beneficial for facilitating the initial step of the AP decomposition reaction. Additionally, the oxidation of NH_3 can further enhance the entropy of the reaction process, thereby increasing gas production and improving the operational capacity of the propellant.

The catalytic reaction mechanism of AP facilitated by energetic complexes can be delineated through the subsequent reaction (4):[46]

$$*R \xrightarrow{-R} * \xrightarrow{+NH_3} *NH_3 \xrightarrow{+OH-H_2O} *NH_2 \xrightarrow{+OH-H_2O} *NH \xrightarrow{+OH-H_2O} *N \xrightarrow{+OH} *NOH \xrightarrow{+OH-H_2O} *NO \xrightarrow{-NO} * + NO \quad (4)$$

In this equation, *R represents the energetic complexes (**ECP-1** to **ECP-4**), while R denotes the ligand associated with the weakest coordination bond, * signifies the complexes after the ligand has dissociated. As shown in Fig. 8, the initial step of the reaction, denoted as *R → *+R, represents the thermal cleavage of the ligand bond within each energetic complex. This process entails a decrease in free energy, aligning consistently with the energy release observed from the decomposition of each

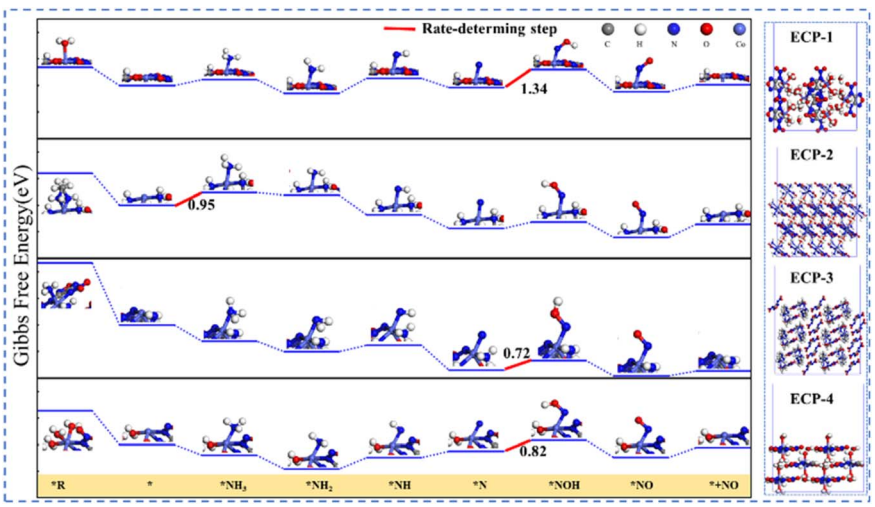

Fig. 8 The Gibbs free energy for the adsorption reaction of NH_3 on **ECP-1** to **ECP-8** (left) and structure optimization model (right).

energetic complex in the DSC data. In the second step of the reaction, indicated as * → *NH_3, where ammonia derived from the decomposition of ammonium perchlorate have been absorbed by the active site. The results display that the Gibbs free energy of **ECP-1** to **ECP-4** of adsorbing NH_3 are 0.45, 0.95, −1.22, −0.80 eV, respectively. It should be noted that for **ECP-1** and **ECP-2**, the adsorption of NH_3 at the active site is characterized as a process that increases free energy, which indicates that in the **ECP-1** and the **ECP-2** systems, the adsorption of NH_3 at the active site does not occur spontaneously. In the context of a complex catalytic reaction, the rate of the overall reaction is frequently determined by the slowest step. This rate-determining step is characterized by the highest energy barrier within the series of reactions involved in the whole process. In the ammonia oxidation process, the highest energy barriers of the rate-determining step are calculated at 1.34, 0.95, 0.72 and 0.82 eV, respectively. Therefore, **ECP-3** has the lowest energy barrier of 0.72 eV, and its decisive step is *N → *NOH, which is calculated to be consistent with the results of AP tests. Furthermore, during the ammonia oxidation process, the maximum energy barriers of the rate-determining steps of **ECP-5** to **ECP-8** were 1.39, 1.19, 1.94 and 1.95 eV respectively, which were far higher than the reaction energy barriers of the Co series complexes. This indicates that the Co series complexes have superior catalytic performance than the Ni series complexes.

Conclusions

This study investigates the modulation of energy and sensitivity of **DNAF** through a coordination strategy, resulting in the synthesis of various energetic metal complexes. The structure and properties of the complex were fully characterized. Experimental findings indicate that the energetic complex strategy significantly enhances the sensitivity (IS ≥ 8 J, FS ≥ 172 N) and thermal stability (T_d ≥ 240 °C) of **DNAF**, with measured densities of **ECP-1** to **ECP-8** are in the range of 1.61–2.11 g cm^{-3}. According to EXPLO5, these energetic complexes have the detonation velocity and detonation pressure values of 6618–8167 m s^{-1} and 16.2–32.0 GPa. Further, catalytic studies have shown that energetic complexes exhibit excellent catalytic efficacy in facilitating the thermal decomposition of AP and boost the burning rate for the HTPB-propellant. The catalytic mechanism was elucidated by density functional theory analysis. **ECP-3** demonstrates a 38% enhancement in the propellant burning rate, positioning it as a potentially effective high-energy catalyst for the thermal decomposition of AP.

Conflicts of interest

There are no conflicts of interest to declare.

Data availability

CCDC 2369080 2369121–2369126 and 2413567 contain the supplementary crystallographic data for this paper.

All data relevant to the work described here are available in the SI. See DOI: https://doi.org/10.1039/d5ta03900b.

Acknowledgements

This work was supported by the National Natural Science Foundation of China (Grant No. 22305122), the Natural Science Foundation of Jiangsu Province (Grant No. BK20230935), the Innovation Foundation of Shanghai Academy of Spaceflight Technology (Grant No. SAST2021-014, SAST2023-079). The authors extend their gratitude to Shiyanjia Lab (https://www.shiyanjia.com) for providing exact test with the XRD analysis. JMS is grateful to the Fluorine-19 fund.

Notes and references

1 J. Zhang, Y. Feng, R. J. Staples, J. Zhang and J. M. Shreeve, *Nat. Commun.*, 2021, **12**, 2146.
2 S. R. Yocca, J. Yount, M. Zeller, E. F. C. Byrd and D. G. Piercey, *Inorg. Chem.*, 2021, **60**, 9645–9652.
3 A. A. Dippold and T. M Klapötke, *J. Am. Chem. Soc.*, 2013, **135**, 9931–9938.
4 D. Fischer, T. M. Klapötke and J. Stierstorfer, *Angew Chem. Int. Ed. Engl.*, 2014, **53**, 8172–8175.
5 P. Wang, Y. Xu, Q. Lin and M. Lu, *Chem. Soc. Rev.*, 2018, **47**, 7522–7538.
6 A. Voronin, I. V. Fedyanin, A. Churakov, A. Pivkina, N. Muravyev, Y. A. Strelenko, M. Klenov, D. Lempert and V. A. Tartakovsky, *ACS Appl. Energy Mater.*, 2020, **3**, 9401–9407.
7 Q. Sun, N. Ding, C. Zhao, J. Ji, S. Li and S. Pang, *Chem. Eng. J.*, 2022, **427**, 130912.
8 T. Liu, S. Liao, S. Song, K. Wang, Y. Jin and Q. Zhang, *Chem. Commun.*, 2019, **56**, 209–212.
9 L. L. Fershtat, *ChemPlusChem*, 2019, **85**, 13–42.
10 A. B. Sheremetev, S. F. Mel'nikova, E. S. Kokareva, R. E. Nekrutenko, K. V. Strizhenko, K. Y. Suponitsky, T. D. Pham, A. N. Pivkina and V. P. Sinditskii, *Defence Technology*, 2021, **18**, 1369–1381.
11 Q. Yu, P. Yin, J. Zhang, C. He, G. H. Imler, D. A. Parrish and J. M. Shreeve, *J. Am. Chem. Soc.*, 2017, **139**, 8816–8819.
12 Y. Tang, J. Zhang, L. A. Mitchell, D. A. Parrish and J. M. Shreeve, *J. Am. Chem. Soc.*, 2015, **137**, 15984–15987.
13 J. T. Lechner, C. Riedelsheimer, S. M. J. Endrass, N. M. Gerold, J. Heidrich, B. Krumm, J. Stierstorfer and T. M. Klapötke, *Chem.–Eur. J.*, 2024, **30**, e202303021.
14 A. K. Yadav, N. Kumar, V. D. Ghule and S. Dharavath, *Org. Lett.*, 2023, **25**, 8606–8610.
15 T. Yan, J. Ma, H. Yang and G. Cheng, *Chem. Eng. J.*, 2022, **429**, 132416.
16 J. Xiong, J. Cai, Q. Lai, P. Yin and S. Pang, *Chem. Commun.*, 2022, **58**, 10647–10650.
17 Y. Oyumi, A. L. Rheingold and T. B. Brill, *J. Phys. Chem.*, 1986, **90**, 4686.
18 R. Wang, Y. Linghu, C. Zhang and K. Zhong, *Hanneng Cailiao*, 2024, **32**, 38–48.
19 V. L. Korolev, T. V. Petukhova, T. S. Pivina, A. B. Sheremetev, E. A. Miroshnichenko and V. P. Ivshin, *Chem. Heterocycl. Compd.*, 2004, **40**, 1568–1587.

20 Y. Zhang, S. Zhang, L. Sun, Q. Yang, J. Han, Q. Wei, G. Xie, S. Chen and S. Gao, *Chem. Commun.*, 2017, **53**, 3034–3037.
21 S. Chen, Y. Jin, H. Xia, K. Wang, Y. Liu and Q. Zhang, *Energ. Mater. Front.*, 2020, **1**, 16–25.
22 T. W. Myers, J. A. Bjorgaard, K. E. Brown, D. E. Chavez, S. K. Hanson, R. J. Scharff, S. Tretiak and J. M. Veauthier, *J. Am. Chem. Soc.*, 2016, **138**, 4685–4692.
23 G. Duan, X. Yang, J. Chen, G. Huang, L. Lu and X. Wang, *Powder Technol.*, 2007, **172**, 27–29.
24 E. Alizadeh-Gheshlaghi, B. Shaabani, A. Khodayari, Y. Azizian-Kalandaragh and R. Rahimi, *Powder Technol.*, 2012, **217**, 330–339.
25 S. G. Hosseini, R. Ahmadi, A. Ghavi and A. Kashi, *Powder Technol.*, 2015, **278**, 316–322.
26 W. Gao, X. Liu, Z. Su, S. Zhang, Q. Yang, Q. Wei, S. Chen, G. Xie, X. Yang and S. Gao, *J. Mater. Chem. A*, 2014, **2**, 11958–11965.
27 Y. Xu, Y. Wang, Y. Zhong, G. Lei, Z. Li, J. Zhang and T. Zhang, *Energ Fuel*, 2020, **34**, 14667–14675.
28 J. Zhang, B. Jin and R. Peng, *Appl. Surf. Sci.*, 2024, **647**, 158970.
29 B. Li, J. Han, Q. Yang, X. Tian and X. Chen, *Z. Anorg. Allg. Chem.*, 2015, **641**, 2371–2375.
30 M. Cibian, S. Derossi and G. S. Hanan, *Dalton Trans.*, 2011, **40**, 1038–1040.
31 T. Zhang, H. Shi, Y. Zhang, Q. Liu, W. Fei and T. Wang, *Appl. Surf. Sci.*, 2021, **552**, 149506.
32 J. B. Zhuo, Z. H. Ma, C. X. Lin, L. L. Xie, S. Bai and Y. F. Yuan, *J. Mol. Struct.*, 2015, **1085**, 13–20.
33 M. Suceska, Explo5 – computer program for calculation of detonation parameters, *2th International Annual Conference of ICT* 2001.
34 T. Wang, X. Wang, Z. Yi, W. Cao, W. Dong, Y. Bi, S. Zhu and J. Zhang, *Cryst. Growth Des.*, 2021, **21**, 7002–7007.
35 J. G. Xu, X. Z. Li, H. F. Wu, F. K. Zheng, J. Chen and G. C. Guo, *Cryst. Growth Des.*, 2019, **19**, 3934–3944.
36 R. R. Sirach and P. N. Dave, *Chem. Heterocycl. Compd.*, 2021, **57**, 720–730.
37 M. A. Spackman and D. Jayatilaka, *CrystEngComm*, 2009, **11**, 19–32.
38 J. Zhang, Q. Zhang, T. T. Vo, D. A. Parrish and J. M. Shreeve, *J. Am. Chem. Soc.*, 2015, **137**, 1697–1704.
39 C. Zhang, Z. Yang, X. Zhou, C. Zhang, Y. Ma, J. Xu, Q. Zhang, F. Nie and H. Li, *Cryst. Growth Des.*, 2014, **14**, 3923–3928.
40 J. L. Arroyo, A. Norambuena, H. Reyes, C. Valdebenito, G. Abarca, D. MacLeod Carey and C. Morales-Verdejo, *Inorg. Chem.*, 2021, **60**, 1436–1448.
41 P. K. Gallagher and D. W. Johnson, *Thermochim. Acta*, 1976, **14**, 255.
42 J. VandeVondele and J. Hutter, *J. Chem. Phy.*, 2007, **127**, 114105.
43 S. Goedecker, J. Hutter and M. Teter, *Phys. Rev. B: Condens. Matter Mater. Phys.*, 1996, **54**, 1703–1710.
44 C. Hartwigsen, S. Goedecker and J. Hutter, *Phys. Rev. B: Condens. Matter Mater. Phys.*, 1998, **58**, 3641–3662.
45 S. Gobi, L. Zhao, B. Xu, U. Ablikim, M. Ahmed and R. I. Kaiser, *Chem. Phys. Lett.*, 2018, **691**, 250–257.
46 S. Wei, Y. Zhang, H. Tan, Z. Xia, L. Zhai, J. Hu, Q. Yang, G. Xie, Z. Chen and S. Chen, *Small*, 2024, **20**, 240071–240072.